Simulation of tidal currents and nonlinear tidal interactions in the Seto Inland Sea, Japan

Guo, Xinyu
Center for Marine Environmental Studies (CMES), Ehime University

Harai, Koichiro
Applied Technology Co., LTD.

Kaneda, Atsushi
Department of Marine Bioscience, Fukui Prefectural University

Takeoka, Hidetaka
Center for Marine Environmental Studies (CMES), Ehime University

Simulation of tidal currents and nonlinear tidal interactions in the Seto Inland Sea, Japan

Xinyu GUO[*1], Koichiro HARAI[*2], Atsushi KANEDA[*3] and Hidetaka TAKEOKA[*1]

E-mail of corresponding author: *guoxinyu@sci.ehime-u.ac.jp*

Abstract

A two-dimensional depth-integrated hydrodynamic model with spatial resolution of 1 km is established and used to calculate the major four tidal constituents and three shallow water tides inside and outside of the Seto Inland Sea (SIS), Japan. Comparisons with observations show good reproduction of the amplitudes and phases of the M_2, S_2, K_1, and O_1 tides and tidal currents. Inside the SIS, large M_4 and MS_4 tides as well as strong tide-induced residual currents are found around the straits and narrow channels; outside of the SIS, a westward residual current is found along the shelf slope. The tide-induced residual currents have apparent fortnightly variations. Inside the SIS, for instance, the tide-induced residual currents around the straits decrease from the spring tide to the neap tide; outside the SIS, the westward residual current along the shelf slope appears at spring tide but disappears at neap tide. Such a well-calibrated tidal model is a necessary step for the success of a circulation modeling in the SIS.

Key words: *tidal currents, tide-induced residual current, Seto Inland Sea, numerical model, fortnightly variation*

1. Introduction

The Seto Inland Sea (SIS) is the largest semi-enclosed sea in Japan (Fig. 1). It is ~500 km in length, 5~50 km in width, and has an average depth of ~40 m. In the SIS, as many as ~600 small islands form complex coastlines and many narrow straits where the tidal current is known to be very strong. The SIS connects to the Pacific through two channels, the Bungo Channel and Kii Channel, and to the Tsushima Strait through a narrow strait, the Kanmon Strait.

The general features of tides in the SIS have been well described (Ogura, 1932; Higo et al., 1980; Yanagi and Higuchi, 1981; Fujiwara, 1981). The predominant tidal constituent in the SIS is the M_2 tide (Yanagi and Higuchi, 1981). The tides from the Pacific enter the SIS mainly through the Bungo and Kii Channels while that from the Kanmon Strait is minor. After passing through the Bungo and Kii Channels, the tides from the Pacific propagate in opposite directions inside the SIS and converge at the Bisan Strait, inducing the largest amplitude in the Hiuchi-Nada.

Based on observed data at 159 stations, Higo et al. (1980) presented a comprehensive report on the tidal currents of the four major constituents (M_2, S_2, K_1, and O_1) of the SIS. They provide maps of the four major tidal currents, and the harmonic constants of tidal currents at 159 stations are also given. With the collection of more observed data, Yanagi and Higuchi (1981) also proposed a map showing the distribution of the amplitude and phase lag of M_2 tidal currents in the SIS.

The complex coastlines and narrow straits in the SIS lead to great spatial variability in the amplitude of tidal currents. In the narrow straits such as the Naruto Strait and Kurushima Strait, the tidal currents can be as strong as 5 m/s. Meanwhile, in the wide sea regions such as the Hiuchi Nada, the tidal currents are as weak as 0.1 m/s. The large spatial variations in the tidal currents in the SIS have been reported to significantly affect the residual currents, material transport and primary production (see Takeoka (2002) for a review).

Because of the important role of tidal currents in the physical background of the SIS (Takeoka, 2002), any simulation of potential environmental problems must include simulation of the tide. Simulation of tides in the SIS, particularly for the entire region, is made difficult by the complex coastlines and narrow straits. The strong tidal currents in the straits also increase the difficulty in achieving model stability.

*1   Center for Marine Environmental Studies (CMES), Ehime University
*2   Applied Technology Co., LTD., Osaka
*3   Department of Marine Bioscience, Fukui Prefectural University

The strong tidal currents around the straits and the large spatial variations in the amplitude of tidal currents indicate the possibility of strong nonlinear tidal interactions in the SIS. Establishment of a calibrated tidal model provides an opportunity to examine nonlinear tidal interactions in the SIS, which have not been sufficiently addressed previously. Tide-induced residual currents in the SIS have been recognized for many years (Oonishi, 1977; Yanagi and Yoshikawa, 1983) yet have not been documented, nor have their fortnightly variations with the spring-neap tidal cycle.

In Section 2, the configuration of the numerical model is briefly described. In Section 3, comparisons of the model results with observations are given. In Section 4, the nonlinear effects including the M_4 and MS_4 tides and tide-induced residual currents are presented. Finally, a short summary is given.
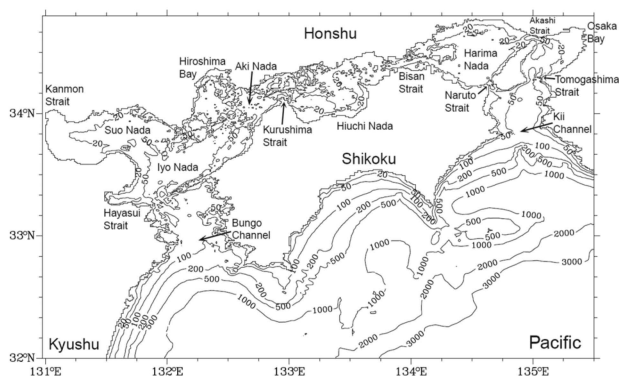

Fig. 1 Model domain and bathymetry. The contour levels are 10, 20, 50, 100, 200, 500, 1000, and 3000 m.

2. Model description

We use a community model, the Princeton Ocean Model (POM, Mellor, 2004), as the base of our simulations. The POM is a three-dimensional primitive equation model that adopts terrain-following coordinates in the vertical. In this application, however, we only use its external mode portion to solve the vertically integrated equations, i.e., to solve a horizontal two-dimensional problem. The vertical structure of tidal currents is beyond our present interests.

The southern boundary of the model is set to 32°N (Fig. 1) because it is also applied to the simulation of residual currents in the SIS, which are affected by the Kuroshio current. The model resolution is roughly 1 km (1/80 degree in the zonal direction and 1/120 degree in the meridional direction). The 250 m digital map data from the Geographical Survey Institute, Japan, are used to form the mode coastline; bathymetry data with 1 km resolution from JODC (Japan Oceanographic Data

Center) are specified at each grid point. Furthermore, depth data from navigational charts are used to modify the model bathymetry inside the SIS (131-135.5°E and 33.8-34.8°N). The final bathymetry and coastline used in the model are shown in Fig. 1, and the minimum water depth is set as 5 m.

The horizontal eddy viscosity is calculated by the Smagorinsky formula in which the proportional factor (HORCON in POM) is set to 0.1. The bottom stresses are calculated using a common quadratic friction law. The drag coefficient is calculated by the embedded formula in the POM (Mellor, 2004), in which the roughness is set to 0.03 cm. The maximum and minimum drag coefficients are set as 0.0075 and 0.0025, respectively.

The model is forced by sea level oscillations along the southern, eastern, and western open boundaries (Fig. 1). In our calculations, we included four major constituents: the M_2, S_2, K_1, and O_1 tides. The harmonic constants of these tidal constituents are available from the results of a regional ocean tide model for the waters around Japan (Matsumoto et al., 2000).

The calculations forced by four tidal constituents were run for 65 days with a time step of 1.5 seconds. The hourly results of the last 60 days were used in the harmonic analysis. In addition to the four major tidal constituents, three shallow water tides (M_4, MS_4, S_4) were also calculated from the output.

3. Results

3.1 Semidiurnal and diurnal tides

Comparison of co-range and co-tidal charts of the M_2 tide from the model results (Fig. 2a) with those given by Yanagi and Higuchi (1981) (not shown here but can be found in Takeoka (2002)) shows that the model well reproduces the general distribution of the M_2 tide. On the open ocean side, the amplitude of the M_2 tide is ~0.45 m and the phase lag is ~180 degrees. On the western side of SIS, after passing the Bungo Channel, the amplitude and phase lag of the M_2 tide increase eastward and reach a maximum (~1.1 m and ~330 degrees, respectively) in the Hiuchi-Nada. On the eastern side, after passing the Kii Channel, the amplitude of the M_2 tide decreases and reaches a minimum (<0.3 m) around the Akashi Strait. From there, it increases westward. After amplification in the Bisan Strait, the amplitude reaches its maximum in the Hiuchi-Nada. Unlike the complex distribution of the amplitude, the phase lag monotonously increases from the Kii Channel to the Hiuchi-Nada. The model also reproduces local features such as the small amplitude on

the western coast of the Bungo Channel, which has been explained as the superposition of Kelvin waves (Yanagi, 1987).

The co-range and co-tidal charts of the K_1 tide (Fig. 2b) show a relatively simple distribution. On the open ocean side, the amplitude and phase lag of the K_1 tide are 0.22 m and ~190 degrees, respectively. After the K_1 tide enters the SIS, the amplitudes and phase lags monotonously increase and reach their maxima in the Hiuchi-Nada. Compared to the semidiurnal tides, the increase of the amplitude and phase lag of the diurnal tides from the open ocean side to the inner part of the SIS is slight.
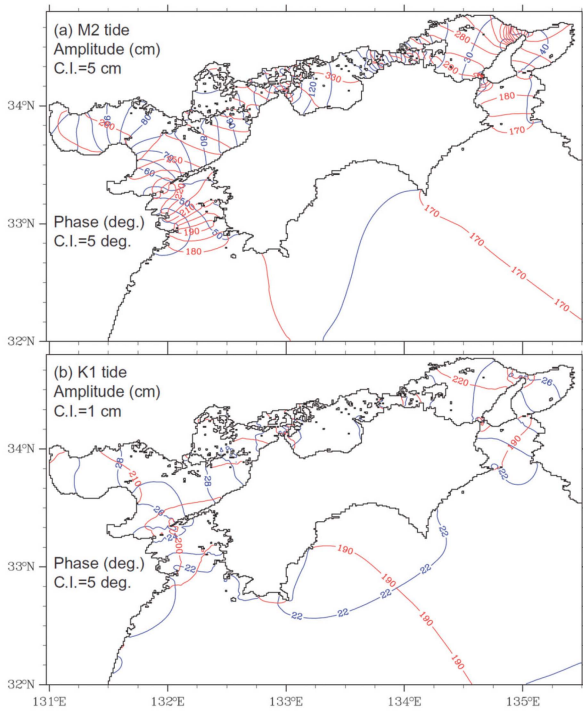

Fig. 2 Co-range (blue lines) and co-tidal (red lines) charts of the (a) M2 tide and (b) K1 tide in the Seto Inland Sea. The phase lag is referenced to 135 E.

In addition to the above qualitative comparisons, quantitative comparisons with the observed data are also necessary to verify the model results. We collected the harmonic constants at 139 tidal gauges located in the model domain (Fig. 3a) from a table of tidal harmonic constants around the Japan coast (Japan Coast Guard, 1992). The root mean square errors of the amplitudes and phase lags are calculated by using the following equations.

$$RMSA = \left[\frac{1}{N} \sum_{k=1}^{N} (A_c^k - A_o^k)^2 \right]^{1/2}$$

(1)

$$RMSP = \left[\frac{1}{N} \sum_{k=1}^{N} (\delta_c^k - \delta_o^k)^2 \right]^{1/2}$$

(2)

Here, A is the amplitude, δ is the phase lag, subscript c denotes the model results, subscript o denotes the observed data, superscript k denotes the tidal gauge data and N is the total number of tidal gauges. Another index giving an overall measure of the model performance (Matsumoto et al., 2000) is calculated by using the following equation.

$$RMS = \left\{ \frac{1}{N} \sum_{k=1}^{N} 0.5 \left[\left(A_c^k \right)^2 - 2 A_c^k A_o^k \cos(\delta_c^k - \delta_o^k) + \left(A_o^k \right)^2 \right] \right\}^{1/2}$$
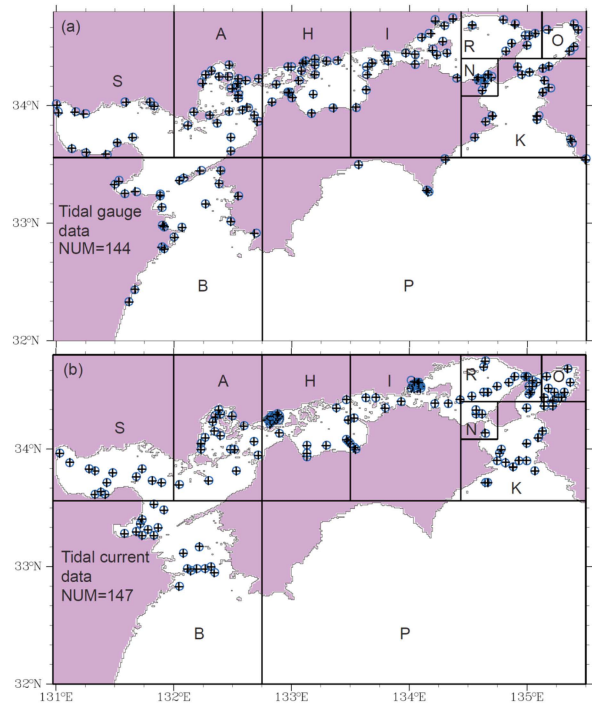
(3)

Fig. 3 Locations of (a) tidal gauges and (b) current meters in the SIS. Open circles denote observation locations and the + symbol inside the open circles denotes the corresponding grid point. Capital letters in each block are used to denote the results by region in Figs. 4 and 6.

In general, the semidiurnal and diurnal tides show good agreement between the model results and observed data at the tidal gauges (Fig. 4). In the case of the semidiurnal tides, RMSA is ~7 cm for the M_2 tide and ~3 cm for the S_2 tide; RMSP is ~18 degrees for the M_2 tide and ~14 degrees for the S_2 tide; RMS is ~8 cm for the M_2 tide and ~3 cm for the S_2 tide. For the diurnal tides, RMSA is ~2 cm for the K_1 tide and ~2 cm for the O_1 tide; RMSP is ~7 degrees for the K_1 tide and ~5 degrees for the O_1 tide; RMS is ~2 cm for the K_1 tide and ~1 cm for the O_1 tide. As an overall evaluation, the relative errors of four major tidal constituents are

roughly within 5 % of their maximum amplitudes.

The capital letters in Fig. 4 represent different regions as shown in Fig. 3a. The model overestimates the amplitude of both the M_2 and S_2 tides in the Hiuchi-Nada, Bisan Strait, and Akashi Strait. The maximum inconsistency reaches 0.2 m for the M_2 tide. On the other hand, the model underestimates the phase lag of the M_2 tide in the Akashi Strait, Bisan Strait, and Naruto Strait. The apparent inconsistency in the diurnal tides is the underestimation of the amplitude of the K_1 tide in the Hiuchi-Nada and Bisan Strait.
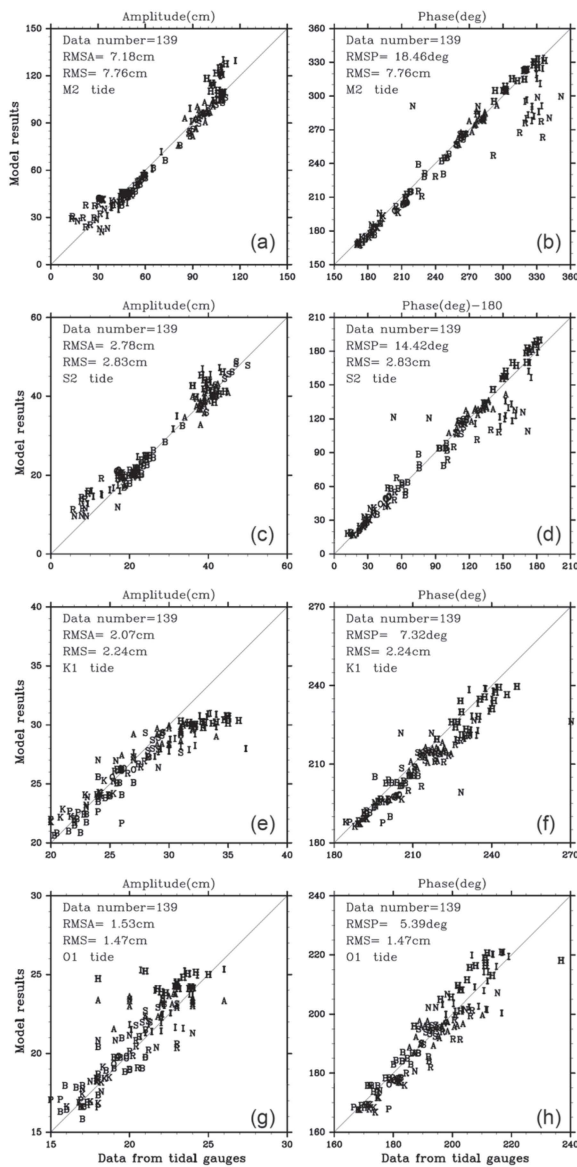
3.2 Semidiurnal and diurnal tidal currents

Maps of the amplitudes of semidiurnal tidal currents and diurnal tidal currents as well as the harmonic constants of observed tidal currents reported by Higo et al. (1980) are used to verify the modeled tidal currents. Although the maps of amplitudes and phase lags of the M_2 tidal current in Yanagi and Higuchi (1981) are similar to those given by Higo et al. (1980), the figures in Higo et al. (1980) give a much finer distribution in some regions, e.g., Osaka Bay.
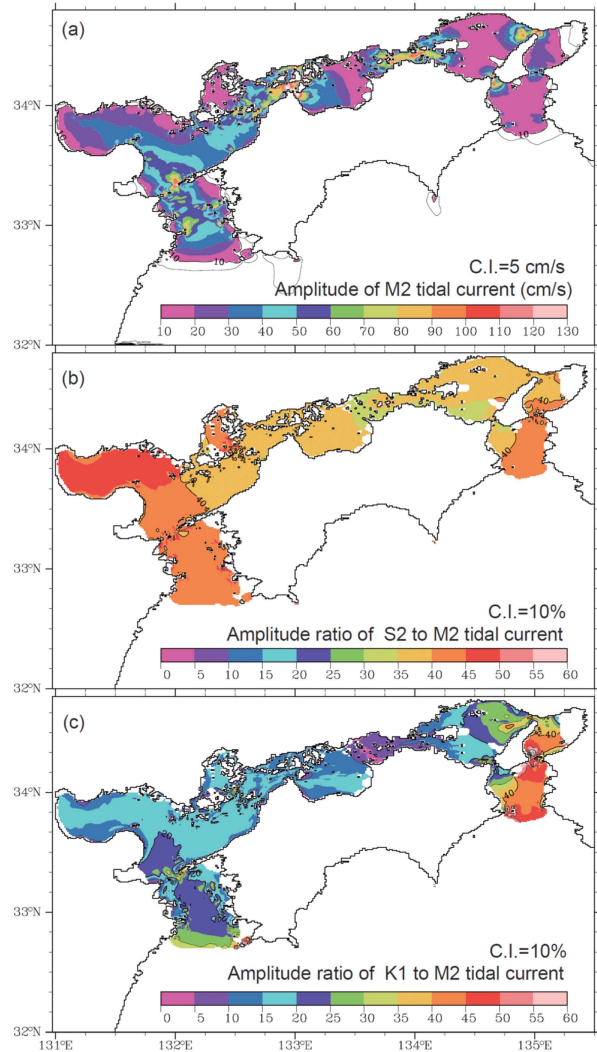

Fig. 5 (a) Amplitude of the M_2 tidal current, (b) ratio of the amplitude of the S_2 tidal current to that of the M_2 tidal current, and (c) ratio of the amplitude of the K_1 tidal current to that of the M_2 tidal current. The ratio was not defined if the amplitude of the M_2 tidal current was smaller than 10 cm/s.

Fig. 4 Comparison of amplitude and phase between model results and harmonic constants at the tidal gauges shown in Fig. 3a for the M_2, S_2, K_1 and O_2 tides. The regions corresponding to the capital letters are shown in Fig. 3a. RMSA, RMSP and RMS are defined by (1)-(3).

The model (Fig. 5a) well reproduces the general distribution of the observed amplitude of the M_2 tidal current (Higo et al., 1980). On the open ocean side, the M_2 tidal currents are weaker than 0.10 m/s. Entering the Bungo Channel and Kii Channel, the tidal currents

become strong, particularly at the straits inside of the SIS. At the Hayasui Strait, Kurushima Strait, Bisan Strait, Akashi Strait, and Naruto Strait, the modeled M_2 tidal currents are over 1 m/s (Fig. 5a), as shown by the observed data (Higo et al., 1980). In the wide sea regions such as Suo-Nada, Hiuchi-Nada, Harima-Nada, and Osaka Bay, the M_2 tidal currents are weak. In general, the M_2 tidal currents are stronger on the western side of the SIS than on the eastern side (Fig. 5a).

The amplitude of the S_2 tidal current is likely in proportion to that of the M_2 tidal current (Fig. 5b). The ratio of amplitudes between two tidal currents ranges between 0.3~0.5, indicating a large fortnightly variation in the SIS. The K_1 tidal current is much weaker than the M_2 tidal current (Fig. 5c). The ratio of amplitudes between two tidal currents is less than 0.25 for the area west of the Akashi Strait, but reaches a value of 0.45 in Osaka Bay and the Kii Channel, where the M_2 tidal current is quite weak.

Quantitative comparisons of the amplitudes of the four major tidal currents between the observed data in Higo et al. (1980) and the model results are given in Fig. 6. At some stations in Higo et al. (1980), the data contains more than one set of harmonic constants. Observations in different periods may present temporal variation in harmonic constants even at the same station, while observations at different depths at the same station also present vertical variation in harmonic constants. To make comparisons possible, we temporally and vertically averaged the data at these stations.

Except for some stations in the straits, the amplitudes of tidal currents for the observed data and model results are consistent. RMSA is ~0.14 m/s for the M_2 tidal current, ~0.06 m/s for the S_2 tidal current, 0.03 m/s for the K_1 tidal current, and ~0.05 m/s for the O_1 tidal current. As an overall evaluation, the relative errors of the four major tidal currents are roughly within 10~15 % of their maximum amplitudes.

The inconsistency between the modeled and observed tidal currents near the straits has two possible causes. One is due to the large spatial gradient of the tidal currents in the straits. A small mismatching of the station position may induce large errors. Another is due to the large lateral variation of the coastline and the steep bathymetry in the straits. It is well known that the tidal current is more sensitive to the local topography than the tidal amplitude. If the model resolution is not sufficient to accurately represent the coastline, the reproduction of tidal currents near to the straits may be poor. Similarly, if the model resolution is not sufficient to represent variations in bathymetry in the straits, the reproduction of tidal currents in the strait may also be

poor. In fact, many straits in the SIS are steep and even narrower than the model resolution. Consequently, the model tends to underestimate tidal currents in the straits.
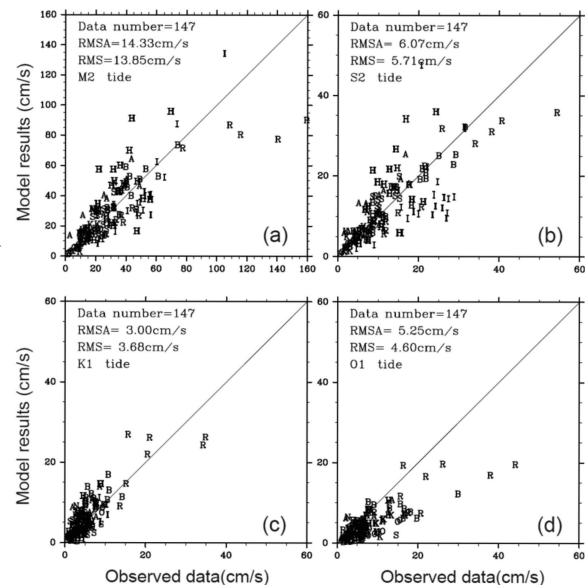

Fig. 6 Comparison of the amplitude of tidal currents between the model results and observed data at the stations shown in Fig. 3b for the M_2, S_2, K_1 and S_2 tides. The capital letters correspond to the regions shown in Fig. 3b. RMSA, RMSP and RMS are defined by (1)-(3).

3.3 Shallow water tides and fortnightly variations of tide-induced residual currents

Nonlinear tidal interactions in shallow waters have been understood for a long time (see Parker (1991) for a review). The nonlinear interactions of an individual tidal constituent produce tide-induced residual currents and overtides; the nonlinear interactions between different tidal constituents produce compound tides and low frequency variations of tide-induced residual currents. In the SIS, the predominant tidal constituent is the M_2 tide and the S_2 tide is secondary. Therefore, the relatively strong shallow water tides in the SIS, i.e., compound tides and overtides, should be the M_4, MS_4 and S_4 tides, and the major low frequency variations of tide-induced residual currents should be fortnightly variations with the spring-neap cycle.

The nonlinear tidal effects are strong in areas with strong tidal currents (Parker, 1991). In the SIS, this corresponds to the narrow straits and some local capes (Misaki in Japanese) where the tidal currents are strong and their spatial gradients are large. The model produces the largest amplitude of the M_4 and MS_4 tides in the Kurushima Strait (Fig. 7), where their observed amplitudes are 8.1 cm and 6.1 cm, respectively. Large amplitudes of the M_4 and MS_4 tides can also be found in

the Hayasui Strait, Aki-Nada, Hiroshima Bay, Bisan Strait, Akashi Strait and Naruto Strait with an order of 2 ~ 6 cm. The S_4 tide (not shown here) is much smaller than the M_4 and MS_4 tides.
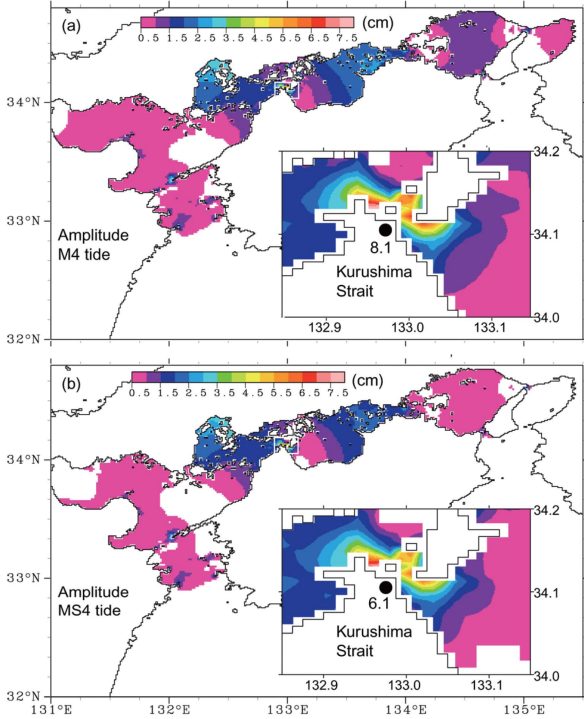
the straits and capes where the amplitudes of the M_4 and MS_4 tides are large. In the Hayasui Strait and Naruto Strait, the M_4 and MS_4 tidal currents are over 0.10 m/s. In the Aki-Nada, Kurushima Strait, Bisan Strait, Akashi Strait, and the vicinity around the capes in the Bungo Channel, the M_4 and MS_4 tidal currents are of the order of 0.02 ~ 0.10 m/s.

As stated before, we are also interested in the tide-induced residual currents and their fortnightly variations. During the model calculation period, there are four spring-neap tide cycles (Fig. 9a). The spring tide at day 30 is the strongest while the neap tide at day 38 is the weakest (Fig. 9b).

Fig. 7 Amplitude of the (a) M_4 and (b) MS_4 tides. The Kurushima Strait is shown in close-up, in which the numbers show the observed amplitude of the corresponding tide (cm).
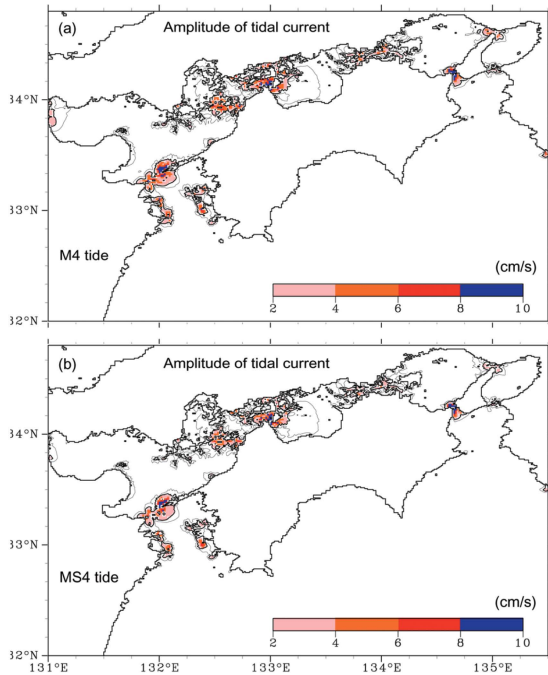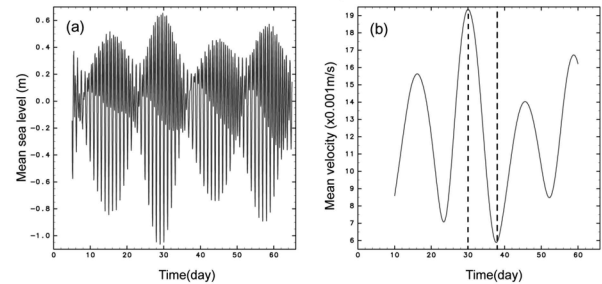

Fig. 9 (a) Hourly mean sea level averaged over the entire model domain, and (b) hourly mean velocity averaged over the entire model domain in which the tidal signals have been filtered out with a 48-hour tide killer filter (Hanawa and Mitsudera, 1985).

Fig. 8 Amplitude of the (a) M_4 and (b) MS_4 tidal currents.

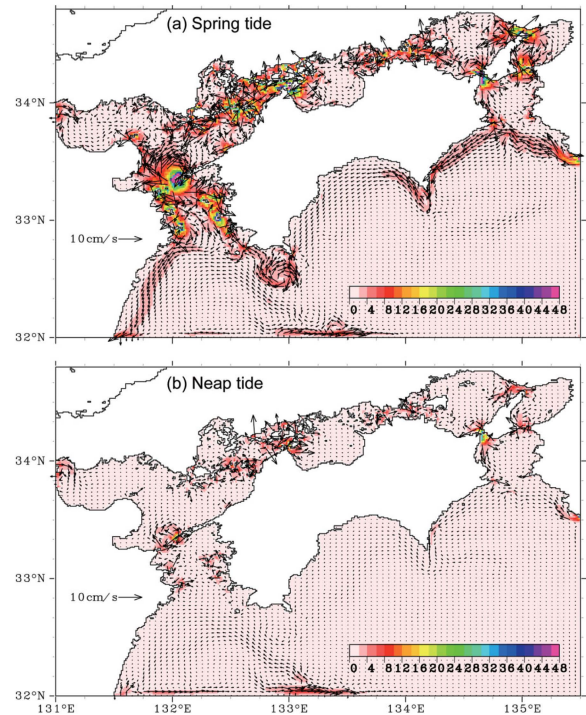The M_4 and MS_4 tidal currents (Fig. 8) are strong in

Fig. 10 Tide-induced residual currents at (a) spring tide and (b) neap tide. The arrows are drawn every four grid points. When the magnitude of the currents is larger than 0.10 m/s, the arrow is not drawn.

The tide-induced residual currents at spring tide (day 30) and at neap tide (day 38) show a sharp contrast in the strength of currents (Fig. 10). Outside the SIS, a westward flow along the shelf slope appears at spring tide but almost disappears at neap tide. This westward current along the shelf slope outside the SIS has not been previously reported. Inside the SIS, the intensity of tide-induced residual currents changes several times over the course of one spring-neap tide cycle. For example, in the vicinity of the Sada Cape in the Hayasui Strait, the tide-induced residual currents vary from ~0.50 m/s at spring tide to ~0.10 m/s at neap tide.

The tide-induced residual currents related to the SIS have been investigated by many studies (Yanagi, 1976; Oonishi, 1977; Yasuda, 1980; Yanagi and Yoshikawa, 1983), mainly with focus on idealized topography or a specific bay like Osaka Bay. These studies have not paid attention to the fortnightly variations of tide-induced residual currents and have not reported on the presence of tide-induced residual currents outside the SIS. However, the generation of tide-induced residual currents over a shelf slope has been recognized (Zhang et al., 1996; Blass and Swart, 2002). Through theoretical analysis and laboratory experiments, Zhang et al. (1996) proposed the generation of mean flows along the depth contours of a shelf slope with the shallow region on the right by the tidal currents propagating normal to the slope. Blass and Swart (2002) confirmed the generation of a mean current by the tidal currents in the presence of density-driven currents and presented its vertical structure in the case of an idealized slope. Considering the topography outside the SIS (Fig. 1) and the distribution of the phase lag of the M_2 tide (Fig. 2), we infer that the westward current along the shelf slope results from the same generation mechanism as proposed by Zhang et al. (1996) and Blass and Swart (2002).

For a better understanding of the tide-induced residual currents inside the SIS, we focus on the tide-induced residual currents in its western portion (Fig. 11) and eastern portion (Fig. 12), respectively. In the western portion (Fig. 11), strong tide-induced residual currents exist in the Hayasui Strait, the vicinity of the capes in the Bungo Channel, the Aki-Nada, and the Kurushima Strait. A clockwise circulation is found north of the Hayasui Strait while an anticlockwise circulation exists south of the Hayasui Strait. The appearance of a pair of eddies is typical of tide-induced residual currents for a topography where a cape extends into a strait (Oonishi, 1977; Imasato, 1983).

The tide-induced residual currents at the south end

of the Bungo Channel are southward and they appear only at spring tide (Fig. 11a). This suggests a possible relation between the tide-induced residual currents and intrusion of oceanic water into the Bungo Channel. The intrusion of warm oceanic water in the surface layer (Kyucho in Japanese; Takeoka et al., 1993) and the intrusion of cold oceanic water in the bottom layer (bottom intrusion; Kaneda et al., 2002) occur mainly at neap tides in the Bungo Channel. Takeoka et al. (2000) attributed the causes of this phenomenon to the change in vertical tidal mixing along with the spring-neap cycle. However, the southward tide-induced residual currents in the Bungo Channel at spring tide actually tend to obstruct the intrusion of oceanic water into the Bungo Channel. Such fortnightly variation in the tide-induced residual current has been recently suggested to be a major factor controlling the oceanic water intrusions in the Bungo Channel (Nagai and Hibiya, 2013).
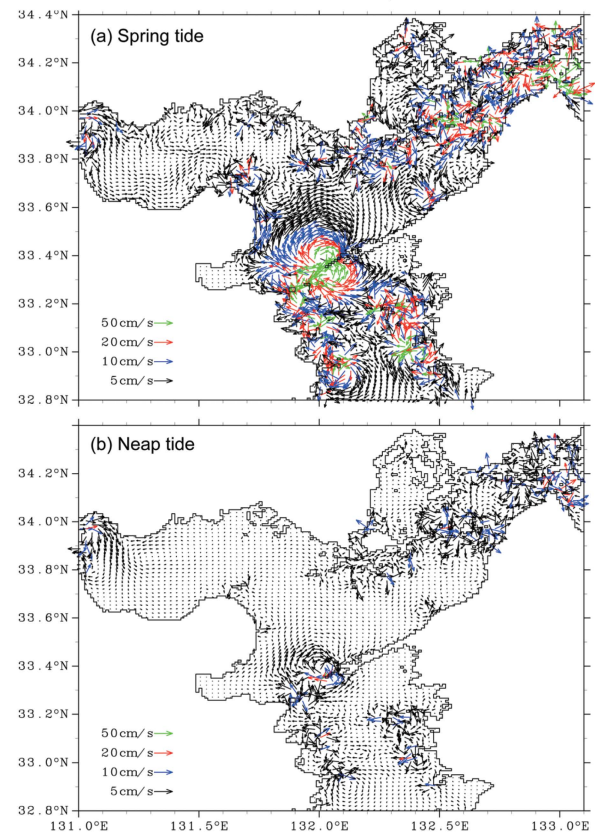

Fig. 11 Tide-induced residual currents at (a) spring tide and (b) neap tide in the western portion of the Seto Inland Sea.

The fortnightly variation in the tide-induced residual current inside the SIS is also strong. An eastward flow along the southern coast of the Suo-Nada can be only found at spring tide (Fig. 11a). The strength of tide-induced residual currents in the Iyo-Nada and

Aki-Nada clearly varies with the spring-neap cycle. A southwestward current offshore of the Iyo-Nada appears only at spring tide. In the Aki-Nada, the tide-induced residual currents are not systematic. This may be related to the model resolution which cannot resolve the islands and straits in the Aki-Nada.
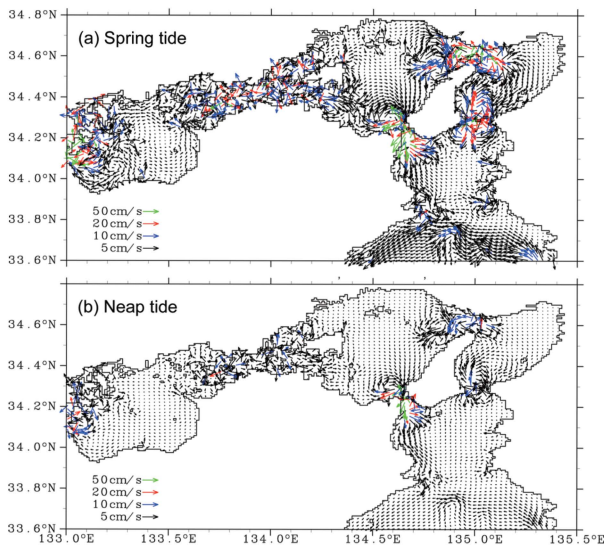

Fig. 12 Tide-induced residual currents at (a) spring tide and (b) neap tide in the eastern portion of the Seto Inland Sea.

In the eastern portion of the SIS (Fig. 12), strong tide-induced residual currents are found around the straits. The fortnightly variation is significant but no residual currents disappear at neap tide. In the western part of the Hichui-Nada, a clockwise circulation is formed next to the outward current in the Kurushima Strait. In the Bisan Strait, the residual currents are strong but not systematic. Between the Bisan Strait and Harima-Nada, eastward currents are formed. North of the Naruto Strait, a clockwise circulation is formed; south of the Naruto Strait, instead of a closed circulation, a southward current is formed. The southward currents extend to outside the Kii Channel along the western coast of the Kii Channel and merge into the westward current along the shelf slope outside of the SIS. Inside the Akashi Strait, the tide-induced residual currents flow both westward to the Harima-Nada and eastward to Osaka Bay; west of the Akashi Strait, two eddies, a large clockwise one at the north and a small anticlockwise one at the south, are formed; east of the Akashi Strait, a large clockwise circulation is formed. North of the Tomogashima Strait, a clockwise circulation is formed; south of the Tomogashima Strait, a pair of eddies, a clockwise one to the west and an anticlockwise one to the east, are formed.

The presence of one or two eddies between a strait and a bay is closely related to the lateral variation of coastline. If there is only one cape extending into the strait while the opposite coastline is straight, only one eddy is formed between the strait and the bay (Oonishi, 1977). If there are two capes extending into the straits from two opposite directions, two eddies appear between the strait and the bay (Imasato, 1983). The circulations north and south of the Hayasui Strait are the typical examples of the one cape case, while the circulation west of the Akashi Strait as well as that south of the Tomogashima Strait correspond to the case of two capes.

The clockwise eddy east of the Akashi Strait in Osaka Bay has been known well from numerical experiments (Oonishi, 1979) and current observations (Fujiwara, 1981). Observations (Fujiwara, 1981) inside the Naruto Strait and Akashi Strait suggest the presence of outward currents from the straits. Observations (Fujiwara, 1981) west of the Akashi Strait indicate a westward current to the middle of the Harima-Nada, an eastward current along northern coast of the Harima-Nada, and a northwestward current along the eastern coast of the Harima-Nada (=west coast of the Awaji Island). Despite the presence of the density or wind driven residual currents in the observed current data, the features of the current field given by Fujiwara (1981) are consistent with the tide-induced residual currents shown in Fig. 12.

4. Summary

Using a two-dimensional depth-integrated model covering the entire SIS in 1 km grid cells, we calculated the four major tidal constituents and three shallow water tides from the simulated time series. The calculated tides and tidal currents of the four major tidal constituents, M_2, S_2, K_1, and O_1, have been compared with observations both qualitatively and quantitatively. The qualitative comparisons show good reproduction of the general patterns of tidal amplitudes and phase lags as well as the amplitudes of tidal currents. The quantitative comparisons with the harmonic constants at 139 tidal gauges show that the relative errors of the model results are within 5 % of the maximum amplitude for the four major tidal constituents; the quantitative comparisons with the amplitudes of tidal currents measured by 147 mooring current meters show a small relative error of 10~15 % of the maximum amplitude of tidal currents.

Nonlinear tidal interactions in the SIS were also examined. Inside the SIS, large M_4 and MS_4 tides as well as strong tide-induced residual currents are found around the straits and narrow channels; outside the SIS,

a westward residual current is found along the shelf slope. The tide-induced residual currents have apparent fortnightly variations. Inside the SIS, for instance, the tide-induced residual currents around the straits decrease from spring tide to neap tide; outside the SIS, the westward residual currents along the shelf slope appear at spring tide but disappear at neap tide.

As shown in Fig. 4, a systematic error can be found in the modeled tides. An example is the overestimation of tides in the Hiuchi-Nada. This could be caused by the poor representation of the topography in the narrow straits such as the Naruto Strait, Akashi Strait, Bisan Strait, and Kurushima Strait. It could also be caused by the poor representation of bottom friction, which may be insufficient to dampen the tidal energy in the Hiuchi-Nada. These two causes, however, are not independent of each other. As shown by Harai et al. (2001), the improvement of horizontal resolution of a tidal model from 1 km to 250 m can decrease the root mean square errors of the M_2 tide inside the SIS by 50 %. The improvement of model resolution not only improves the representation of the coastline and bathymetry, but also improves the representation of bottom friction because a fine grid model simulates more accurate tidal currents, particularly in narrow straits (Harai et al., 2001).

The underestimation of tidal currents in the narrow straits (Fig. 6) may mean that the nonlinear tidal effects in the SIS could also be underestimated. Therefore, although we have shown strong nonlinear tidal interactions in the SIS, the real situation could be stronger than those presented here. The nonlinear tidal interactions not only influence the tides and tidal currents, but also cause fortnightly variations in the residual currents. They can naturally induce fortnightly variations in water temperature and salinity fields. Therefore, the simulations for the density-driven current must consider the spring-neap tidal cycle.

Since the tidal currents determine the background for the vertical mixing, a well calibration for tidal model, in particular that for the tidal currents, is a necessary step for the success of a circulation modeling in the SIS (Chang et al., 2009).

References

Blaas, M., and H. B. de Swart (2002): Vertical structure of residual slope circulation driven by JEBAR and tides: an idealized model. *Cont. Shelf Res.*, **22**, 2687-2706.

Chang, P.-H., X. Guo, and H. Takeoka (2009): A numerical study on the seasonal circulation in the Seto Inland Sea, Japan. *J. Oceanogr.*, **65**, 721-736.

Fujiwara, T. (1981): Water exchange in the Seto Inland Sea. *Umi no Kisyou*, **27**, 1-19 (in Japanese).

Hanawa, K., and H. Mitsudera (1985): On daily average of oceanographic data. *Coastal Oceanogr. Bull.*, **23**, 79-87.

Harai, K., X. Guo, and H. Takeoka (2001): A tide model for Seto Inland Sea, Japan (II). *Abstract of 2001 fall meeting of The Oceanogr. Soc. Japan*, 412.

Higo, T., Y. Takasugi, H. Tanabe (1980): Tidal current in the Seto Inland Sea. *Reports of Chugoku National Industrial Research Institute*, **12**, 81-120 (in Japanese).

Imasato, N. (1983): What is tide-induced residual current? *J. Phys. Oceanogr.*, **13**, 1307-1317.

Japan Coast Guard (1992): Table of tidal harmonic constants around Japan coast, publication No.742, Hydrographic and Oceanographic Department.

Kaneda, A., H. Takeoka, E. Nagaura, and Y. Koizumi (2002): Periodic Intrusion of Cold Water from the Pacific Ocean into the Bottom Layer of the Bungo Channel in Japan. *J. Oceanogr.*, **58**, 547-556.

Matsumoto, K., T., Takanezawa, and M. Ooe (2000): Ocean tide models developed by assimilating TOPEX/POSEIDON Altimeter data into hydrodynamical model: a global model and a regional model around Japan. *J. Oceanogr.*, **56**, 567-581.

Mellor, G. L. (2004): User's guide for a three-dimensional, primitive equation, numerical ocean model, *Program in Atmospheric & Oceanic Sciences report*, Princeton University, 41 pp.

Nagai, T., and T. Hibiya (2013): Effects of tidally induced eddies on sporadic Kuroshio-water intrusion (kyucho). *J. Oceanogr.*, **69**, 369-377.

Ogura, S. (1932): The tides in the seas adjacent to Japan. *Bull. Hydrogr. Dep.*, **7**, 1-189.

Oonishi, Y. (1977): A numerical study on the tidal residual flow. *J. Oceanogr. Soc. Japan*, **33**, 207-218.

Oonishi, Y. (1979): Numerical experiments on the constant flow in Osaka Bay. *Proc. of 26th Conf. On Coastal Eng. in Japan*, 514-518 (in Japanese).

Parker, B. B. (1991): Tidal Hydrodynamics. John Wiley

& Sons, Inc, 883 pp.

Takeoka, H. (2002): Progress in Seto Inland Sea Research. *J. Oceanogr.*, **58**, 93-107.

Takeoka, H., H. Akiyama, and T. Kikuchi (1993): The kyucho in the Bungo Channel, Japan - Periodic intrusion of oceanic warm water. *J. Oceanogr.*, **49**, 369-382.

Takeoka, H., Koizumi Y., Kaneda, A. (2000): Year-to-year variation of a kyucho and a bottom intrusion in the Bungo Channel, Japan. *Interactions between Estuaries, Coastal Seas and Shelf Seas*, T. Yanagi, Ed., Terra Scientific Publishing Company (TERRAPUB), 197-215.

Yanagi, T. (1976): Fundamental study on the tidal residual circulation, 1. *J. Oceanogr. Soc. Japan*, **32**, 199-208.

Yanagi, T. (1987): Kelvin wave reflection with phase lag in the Bungo Channel. *J. Oceanogr. Soc. Japan*, **43**, 377-382.

Yanagi, T., and H. Higuchi (1981): Tide and tidal current in the Seto Inland Sea. *Proc. of 28th Conf. On Coastal Eng. in Japan*, 555-558(in Japanese).

Yanagi, T., and K. Yoshikawa (1983): Generation mechanisms of tidal residual circulation. *J. Oceanogr. Soc. Japan*, **39**, 156-165.

Yasuda, H. (1980): Generation mechanism of the tidal residual current due to the coastal boundary layer. *J. Oceanogr. Soc. Japan*, **35**, 241-252.

Zhang, X., D. L. Boyer, N. Perenne, and D. P. Renouard (1996): Mean flow generation along a sloping region in a rotating homogeneous fluid. *J. Geophys. Res.*, **101**, 28597-28614.